Frequency spectrum of second-harmonic radiation excited by a Gaussian Schell-model beam

V. Pyragaite,* A. Stabinis, and A. Piskarskas
Department of Quantum Electronics, Vilnius University, Sauletekio Avenue 9, Building 3, LT-10222 Vilnius, Lithuania
(Received 15 June 2012; published 10 September 2012)

The second harmonic (SH) radiation excited in a nonlinear crystal by a Gaussian Schell-model beam with a broad frequency spectrum is analyzed. It is revealed that the frequency spectrum of the SH wave generated depends on the bandwidth of the angular spectrum of the incoherent fundamental wave as well as on its beamwidth. The influence of the fundamental wave beamwidth on the SH wave intensity is discussed. Analytical treatments and numerical simulations of the nonlinear coupling equations are both presented.

DOI: 10.1103/PhysRevA.86.033812 PACS number(s): 42.25.Kb, 42.65.Ky

I. INTRODUCTION

The first experimental demonstrations of second harmonic (SH) generation from incoherent light were performed in the early works of McMahon and Franklin [1–3]. Recently, the detectable SH radiation of continuous-wave incoherent sources has been demonstrated starting with a microscopic-size light-emitting diode chip, all the way up to distant objects such as the Sun [4]. The coherence properties of an SH beam generated by a monochromatic partially coherent pump were analyzed by the authors of Refs. [5–7], and it was shown that, under certain conditions, the conversion efficiency of the SH beam can be significantly increased up to a factor of 2, as compared to a coherent beam. In the last decade, the idea of incoherent excitation of nonlinear optical processes has resulted in several interesting theoretical works. It was shown that a coherent signal can be generated from an incoherent pump wave in the parametric generation process [8–10]. In this interaction, the idler wave remains incoherent, and the process takes place if the group velocities of two incoherent waves, pump and idler, are the same and differ from the signal wave group velocity. Afterwards, it was revealed that the generation of a coherent wave by two incoherent waves with a continuous spatial-temporal spectrum is possible in a quadratic nonlinear medium when the angular dispersion of both incoherent waves is properly chosen [11]. Experimental work [12] has demonstrated that spatial as well as temporal walk-off effects in a nonlinear crystal can result in an angular dispersion of SH radiation excited by an incoherent pump. In general, the width of the SH frequency spectrum is significantly influenced by the spatial incoherence of the fundamental wave.

In this paper, we present a detailed analysis of the frequency spectrum of the SH radiation excited by an incoherent pump. In the time domain, the fundamental wave is assumed to be a stationary random process. On the other hand, we assume that in the space domain, the fundamental beam is partially coherent and obeys a Gaussian Schell (GS) model [13]. We obtain that the SH frequency spectrum narrows with a propagation through nonlinear medium, and it is revealed that the frequency bandwidth depends on the bandwidth of the angular spectrum of the incoherent fundamental beam as well as on its beamwidth. In the case of a wide angular spectrum, the faster narrowing of the SH frequency spectrum is obtained for smaller beamwidths of the fundamental wave.

The paper is organized as follows. The nonlinear coupling equations and pump wave model are presented in Sec. II. In Sec. III we solve the equations at low conversion efficiency, and the results obtained from numerical calculations as well as those of analytical consideration are presented in Secs. IV and V. In Sec. VI the method utilized for the numerical simulation of the nonlinear coupling equations for the input GS model beam is provided. Finally, the conclusions are drawn in Sec. VII.

II. NONLINEAR COUPLING EQUATIONS

Let us consider the second harmonic generation (SHG) resulting from the GS model beam. In the case of type-I noncritical phase-matching the nonlinear coupling equations for fields $A_j(t,x,z)$ read [14]

$$\frac{\partial A_1}{\partial z} = i\frac{g_{10}}{2}\frac{\partial^2 A_1}{\partial t^2} - \frac{i}{2k_{10}}\frac{\partial^2 A_1}{\partial x^2} - \sigma_1 A_1^* A_2, \tag{1a}$$

$$\frac{\partial A_2}{\partial z} = -\nu\frac{\partial A_2}{\partial t} + i\frac{g_{20}}{2}\frac{\partial^2 A_2}{\partial t^2} - \frac{i}{2k_{20}}\frac{\partial^2 A_2}{\partial x^2} + \sigma_2 A_1^2, \tag{1b}$$

where the indices $j = 1,2$ stand for the fundamental and SH waves, respectively. The central frequencies of the waves obey the relation $\omega_{20} = 2\omega_{10}$, k_{j0}, $g_{j0} = (d^2k_j/d\omega_j^2)_{\omega_{j0}}$ are the wave number ($k_{20} = 2k_{10}$) and group velocity dispersion coefficient at the central frequency, respectively. $u_{j0} = [(dk_j/d\omega_j)_{\omega_{j0}}]^{-1}$ is the group velocity, $\nu = \frac{1}{u_{20}} - \frac{1}{u_{10}}$ is the walk-off parameter, $\sigma_j = d_{\mathrm{ef}}\omega_{j0}^2/(2c^2k_{j0})$ is the coupling coefficient, d_{ef} is the effective quadratic susceptibility, and c is the speed of light. x and z are Cartesian coordinates, and t is time. For simplicity one transverse coordinate (y) was omitted.

Equations (1a) and (1b) can be solved analytically for low conversion efficiency when the nonlinear term in Eq. (1a) can be neglected. The solutions are found for spectral amplitudes $a_j(\Omega,p)$ which are a two-dimensional Fourier transform of the fields $A_j(t,x)$

$$a_j(\Omega,p) = \int_{-\infty}^{\infty}\int_{-\infty}^{\infty} A_j(t,x)\exp[-i(\Omega t - px)]dtdx, \tag{2}$$

here $\Omega = \omega_j - \omega_{j0}$ is the frequency shift with respect to the central frequency, and p is a transverse wave vector. On the other hand, the fields $A_j(t,x)$ are an inverse Fourier transform

*viktorija.pyragaite@ff.vu.lt

of the spectral amplitudes $a_j(\Omega,p)$

$$A_j(t,x)=\frac{1}{4\pi^2}\int_{-\infty}^{\infty}\int_{-\infty}^{\infty}a_j(\Omega,p)\exp[i(\Omega t-px)]d\Omega dp. \tag{3}$$

We assume that at the input of a nonlinear medium ($z=0$) the field of the incoherent fundamental wave is $A_{10}(t,x)$, and its correlation function has the form

$$\begin{aligned}&\langle A_{10}(t_1,x_1)A_{10}^*(t_2,x_2)\rangle\\&\quad=a_0^2\exp\left(-\frac{(t_2-t_1)^2}{\tau^2}\right)\exp\left(-\frac{(x_1+x_2)^2}{4d_0^2}\right)\\&\qquad\times\exp\left(-\frac{(x_2-x_1)^2}{d_1^2}\right).\end{aligned} \tag{4}$$

So we assume that in the time domain, the fundamental wave is a stationary one, and τ is the correlation time. On the other hand, in the space domain, the fundamental beam is partially coherent and obeys the GS model [13]. Here d_0 is the beam radius and $d_1\ll d_0$ stands for the correlation radius. Then, by use of Eq. (2), the correlation function of the spectral amplitude $a_{10}(\Omega,p)$ of the fundamental wave at the input of the nonlinear medium can be written as

$$\begin{aligned}&\langle a_{10}(\Omega_1,p_1)a_{10}^*(\Omega_2,p_2)\rangle\\&\quad=\frac{16\pi^{5/2}a_0^2}{\Delta\Omega_1\Delta\beta_0\Delta\beta_1}\exp\left(-\frac{\Omega^2}{\Delta\Omega_1^2}\right)\exp\left(-\frac{(p_1-p_2)^2}{\Delta\beta_0^2}\right)\\&\qquad\times\exp\left(-\frac{(p_1+p_2)^2}{4\Delta\beta_1^2}\right)\delta(\Omega_1-\Omega_2).\end{aligned} \tag{5}$$

Here $\Delta\Omega_1=\frac{2}{\tau}$ is the frequency bandwidth of the fundamental wave $\Delta\beta_0=\frac{2}{d_0}$ and $\Delta\beta_1=\frac{2}{d_1}$. In general, the spectral amplitude $a_{10}(\Omega,p)$ obeys Gaussian statistics, and the components of the frequency spectrum are δ correlated.

III. SOLUTION OF THE NONLINEAR COUPLING EQUATIONS

We assume that the nonlinear term in Eq. (1a) can be neglected. This assumption is correct when the conversion efficiency in a SHG process is rather low. The Fourier transform of Eqs. (1a) and (1b) gives

$$\frac{\partial a_1}{\partial z}=-i\Delta_1 a_1, \tag{6a}$$

$$\frac{\partial a_2}{\partial z}=-i\Delta_2 a_2+\sigma_2 T, \tag{6b}$$

where $\Delta_1=\frac{g_{10}}{2}\Omega^2-\frac{p^2}{2k_{10}}$, $\Delta_2=\nu\Omega+\frac{g_{20}}{2}\Omega^2-\frac{p^2}{2k_{20}}$, and $T(\Omega,p)=\int_{-\infty}^{\infty}\int_{-\infty}^{\infty}A_1^2(t,x)\exp[-i(\Omega t-px)]dtdx$. The solutions of Eqs. (6a) and (6b) are

$$a_1(\Omega,p)=a_{10}(\Omega,p)\exp[-i\Delta_1(\Omega,p)z], \tag{7a}$$

$$\begin{aligned}a_2(\Omega,p)&=\sigma_2\exp[-i\Delta_2(\Omega,p)z]\\&\quad\times\int_0^z\exp[i\Delta_2(\Omega,p)z]T(\Omega,p,z)dz.\end{aligned} \tag{7b}$$

Making use of Eq. (3), Eq. (7b) can be written in the form

$$\begin{aligned}a_2(\Omega,p)&=\frac{\sigma_2}{4\pi^2}\exp(-i\Delta_2 z)\int_{-\infty}^{\infty}\int_{-\infty}^{\infty}\exp(-iF)\frac{\sin F}{F}\\&\quad\times a_{10}(\Omega_1,p_1)a_{10}(\Omega-\Omega_1,p-p_1)d\Omega_1dp_1,\end{aligned} \tag{8}$$

where

$$F=\frac{z}{2}[\Delta_1(\Omega_1,p_1)+\Delta_1(\Omega-\Omega_1,p-p_1)-\Delta_2(\Omega,p)]. \tag{9}$$

Next, taking into account that the spectral amplitude $a_{10}(\Omega,p)$ obeys Gaussian statistics, we find the correlation function $\langle a_2(\Omega,p)a_2^*(\Omega',p')\rangle$ of the SH radiation. Here we have omitted the rather long calculations and only present the final result

$$\begin{aligned}\langle a_2(\Omega,p)a_2^*(\Omega',p')\rangle&=\frac{32\pi a_0^4\sigma_2^2z^2}{\Delta\Omega_1^2\Delta\beta_0^2\Delta\beta_1^2}\exp\left(i\frac{\alpha(p^2-p'^2)}{2k_{10}^2}-\frac{\Omega^2}{2\Delta\Omega_1^2}-\frac{(p-p')^2}{2\Delta\beta_0^2}-\frac{(p+p')^2}{8\Delta\beta_1^2}\right)\delta(\Omega-\Omega')\\&\quad\times\int_{\Omega_1}\int_{p_1}\int_{p_2}\operatorname{sinc}F_1(\Omega_1,p_1)\operatorname{sinc}F_2(\Omega_1,p_2)\exp\left(i\frac{\alpha\left(p_1^2-p_2^2\right)}{k_{10}^2}\right)\\&\quad\times\exp\left(-2\frac{\Omega_1^2}{\Delta\Omega_1^2}-2\frac{(p_1-p_2)^2}{\Delta\beta_0^2}-\frac{(p_1+p_2)^2}{2\Delta\beta_1^2}\right)d\Omega_1dp_1dp_2,\end{aligned} \tag{10}$$

where $\operatorname{sinc}F=\frac{\sin F}{F}$ and

$$F_{1,2}(\Omega_1,p_{1,2})=\alpha\left[\frac{g_{10}}{k_{10}}\Omega_1^2-\frac{p_{1,2}^2}{k_{10}^2}+h(\Omega)\right]. \tag{11}$$

Here $\alpha=\frac{k_{10}z}{2}=\frac{\pi n_{10}z}{\lambda_{10}}$ is the normalized propagation length. λ_{10} and n_{10} are the wavelength and the refraction index of the fundamental wave, respectively, and $h(\Omega)=-\frac{\nu\Omega}{k_{10}}+\frac{g_{10}\Omega^2}{4k_{10}}-\frac{g_{20}\Omega^2}{2k_{10}}$. Further we introduce into consideration the nonlinear length of interaction

$$L_n=\frac{1}{\sigma_2\sqrt{\langle|A_{10}(0,0)|^2\rangle}}=\frac{1}{\sigma_2 a_0}, \tag{12}$$

see Eq. (4). Then the normalized spectral radiance $G_2(\Omega,p)=\frac{\langle|a_2(\Omega,p)|^2\rangle}{\langle|a_{10}(0,0)|^2\rangle}$ of the SH radiation can be written as

$$\begin{aligned}G_2(\Omega,p)&=\frac{2(z/Ln)^2}{\pi^{3/2}\Delta\Omega_1\Delta\beta_0\Delta\beta_1}\exp\left(-\frac{\Omega^2}{2\Delta\Omega_1^2}-\frac{p^2}{2\Delta\beta_1^2}\right)\\&\quad\times\int_{\Omega_1}\int_{p_1}\int_{p_2}\operatorname{sinc}F_1\operatorname{sinc}F_2\exp\left(\frac{i\alpha\left(p_1^2-p_2^2\right)}{k_{10}^2}\right)\\&\quad\times\exp\left(-2\frac{\Omega_1^2}{\Delta\Omega_1^2}-2\frac{(p_1-p_2)^2}{\Delta\beta_0^2}-\frac{(p_1+p_2)^2}{2\Delta\beta_1^2}\right)\\&\quad\times d\Omega_1dp_1dp_2.\end{aligned} \tag{13}$$

It is obvious that the bandwidth of the angular spectrum of the SH wave exceeds the bandwidth of the fundamental wave by a factor of $\sqrt{2}$, and does not depend on the propagation length. This is caused by noncritical type-I phase matching which was assumed in the consideration. In the case of critical phase matching the angular dispersion of the SH radiation appears [12].

We note that the radiance of the SH radiation generated by the GS model beam depends on the beam radius ($d_0 = \frac{2}{\Delta\beta_0}$) of the fundamental wave also via the exponent $\exp(i\alpha\frac{p_1^2-p_2^2}{k_{10}^2})$ in the integral (13). At $d_0 \to \infty$, $\Delta\beta_0 \to 0$, $p_1 \approx p_2$, $\exp(i\alpha\frac{p_1^2-p_2^2}{k_{10}^2}) \to 1$, and the dependence of the radiance $G_2(\Omega, p)$ on $\Delta\beta_0$ disappears.

IV. SPECTRAL RADIANCE AND FREQUENCY BANDWIDTH OF THE SECOND HARMONIC RADIATION

Here we make use of Eq. (13) and calculate the spectral radiance $G_2(\Omega, p)$ and frequency bandwidth $\Delta\Omega_2$ of the SH radiation. The calculations were performed for an Lithium triborate (LBO) crystal in the case of noncritical type-I phase matching in the x direction ($\theta = 90^\circ, \varphi = 0^\circ$) at a temperature of 387 K for a fundamental wavelength of $\lambda_{10} = 1.1\ \mu$m. The Sellmeier equations from Ref. [15] were adopted. In further consideration, the normalized quantities $a = \frac{\Delta\Omega_1}{\omega_{10}}$, $b_0 = \frac{\Delta\beta_0}{k_{10}}$, $b_1 = \frac{\Delta\beta_1}{k_{10}}$, $r = \frac{ma}{b_1}$, $\delta = \alpha b_0 b_1$, $\mu = \alpha b_0^2$ were introduced, here $m = \sqrt{\omega_{10}^2 g_{10}/k_{10}} \approx 0.063$. The normalized frequency bandwidth a of the fundamental wave was fixed to 0.1. The parameters b_0 and b_1 ($b_0 \ll b_1$) characterize the beamwidth and the angular spectrum of the GS model beam, respectively. The parameter μ can be rewritten as $\mu = \alpha b_0^2 = z/L_d$, where $L_d = \frac{k_{10}d_0^2}{2} = \frac{\lambda_{10}}{\pi n_{10} b_0^2}$ is a Rayleigh length of a coherent Gaussian beam with a beam radius of d_0. So, the quantity μ characterizes the GS model beam envelope diffraction. By use of the approximation $\sin F/F \approx \exp(-\kappa^2 F^2)$, $\kappa \approx 0.41$, for $\alpha \gg 1$ and $\mu \ll 1$ it is possible to simplify the integral (13). As a result, for a spectral radiance of $G_{20} = G_2(0,0)$ we find

$$G_{20} = \frac{(z/Ln)^2}{\sqrt{2}\pi}\int_{-\infty}^{\infty}\int_{-\infty}^{\infty}\frac{\exp\left\{-\xi^2\left[1+\delta^2/\left(4R_1^2\right)\right]-\eta^2-\frac{1}{2}\kappa^2\alpha^2 b_1^4(\xi^2-r^2\eta^2)^2\right\}}{R_1(\xi,\eta)}d\xi\, d\eta, \tag{14}$$

where $R_1(\xi,\eta) = \sqrt{1+\frac{\kappa^2\delta^2}{4}(3\xi^2 - r^2\eta^2)}$. Further the Eq. (14) obtained is used for the analytical evaluation of the spectral radiance G_{20}. The dependence of the spectral radiance G_{20} on the propagation length z in a nonlinear medium was obtained by the numerical calculation of Eq. (13) and is presented in Fig. 1. In the limit case $z \to 0$ ($\alpha \to 0$, $\delta \to 0$, $R_1 \to 1$) the dependence of the radiance with z is quadratic, $G_{20} \approx \frac{1}{\sqrt{2}}(\frac{z}{L_n})^2$. In general, the variation of radiance depends with a propagation on the quantities δ, r, and μ. When $\delta \ll 1$, $r \gg 1$ we have $R_1 \approx 1$, and

$$G_{20} \approx \sqrt{\frac{2}{\pi}}\left(\frac{z}{L_n}\right)^2\int_0^{\infty}\exp(-\eta^2-\varepsilon_1\eta^4)d\eta, \tag{15}$$

where $\varepsilon_1 = \frac{1}{2}\kappa^2\alpha^2 m^2 a^2$. The integration in Eq. (15) gives

$$G_{20} = \frac{1}{4}\sqrt{\frac{2}{\pi}}\left(\frac{z}{L_n}\right)^2\frac{\exp(1/(8\varepsilon_1))}{\sqrt{\varepsilon_1}}K_{\frac{1}{4}}\left[\frac{1}{8\varepsilon_1}\right], \tag{16}$$

where K is the modified Bessel function. So, the radiance depends on the bandwidth of the frequency spectrum but does not depend on the bandwidth of the angular spectrum of the fundamental wave. In this case the spatial coherence of the fundamental wave is rather high, curve 1 in Fig. 1(a). The dependence of the radiance on the parameter b_1 appears when b_1 increases. For example, at $\delta \leqslant 1$, $r \leqslant 1$, Eq. (14) can be written as

$$G_{20} \approx \sqrt{\frac{2}{\pi}}\left(\frac{z}{L_n}\right)^2\int_0^{\infty}\exp(-\xi^2-\varepsilon_2\xi^4)d\xi, \tag{17}$$

where $\varepsilon_2 = \frac{1}{2}\kappa^2\alpha^2 b_1^4$. The integration in Eq. (17) again gives Eq. (16) but with ε_1 changed to ε_2. If $\varepsilon_2 \gg 1$, then $G_{20} \approx \frac{2^{3/4}\Gamma(\frac{1}{4})(\frac{z}{Ln})^2}{4\sqrt{\pi\kappa\alpha b_1}}$, where Γ is the gamma function. The radiance depends on the propagation length z as $z^{3/2}$ and decreases with an increase in b_1, Fig. 1(b), curve 1. The influence of the beam envelope diffraction parameter μ on radiance with propagation is rather weak at $\delta \leqslant 1$, compare curves 2 ($\delta = 0.05$, $\mu = 5\times10^{-4}$) and 3 ($\delta = 0.5$, $\mu = 0.05$) in Fig. 1(a) at $z/L_n = 0.5$ ($\alpha \approx 5\times10^4$). This influence becomes noticeable at $\delta \gg 1$, $\mu > 1$, curves 4 ($\delta = 1.25$, $\mu = 0.0125$) and 5 ($\delta = 12.5$, $\mu = 1.25$) in Fig. 1(a), and is significant at $\mu \gg 1$, curves 2 ($\delta = 5$, $\mu = 0.05$) and 3 ($\delta = 50$, $\mu = 5$) in Fig. 1(b) at $z/L_n = 0.5$.

The frequency spectrum of the SH radiation is shown in Figs. 2 and 3. Here the frequency spectrum is normalized to its peak value. When the beamwidth of the fundamental wave is rather large [$b_0 = 10^{-4}$, Fig. 2(a)], the bandwidth of the frequency spectrum significantly depends on the angular bandwidth of the fundamental wave. In this case, the influence of the envelope of the fundamental beam can be neglected, and the frequency bandwidth of the SH radiation increases with an increase in the angular bandwidth of the fundamental wave (parameter b_1). This is caused by the possibility for different frequency components to obey better noncollinear phase-matching conditions when the angular spectrum is broad. The influence of the angular spectrum of the fundamental beam on the frequency bandwidth of the SH radiation becomes insignificant at $b_1 < 0.01$, Fig. 2(b). At $b_0 \to 0$, $b_1 \to 0$ and $b_0 \ll b_1$, $\exp(-2\frac{(p_1-p_2)^2}{\Delta\beta_0^2}) \to \sqrt{\frac{\pi}{2}}\Delta\beta_0\delta(p_1-p_2)$,

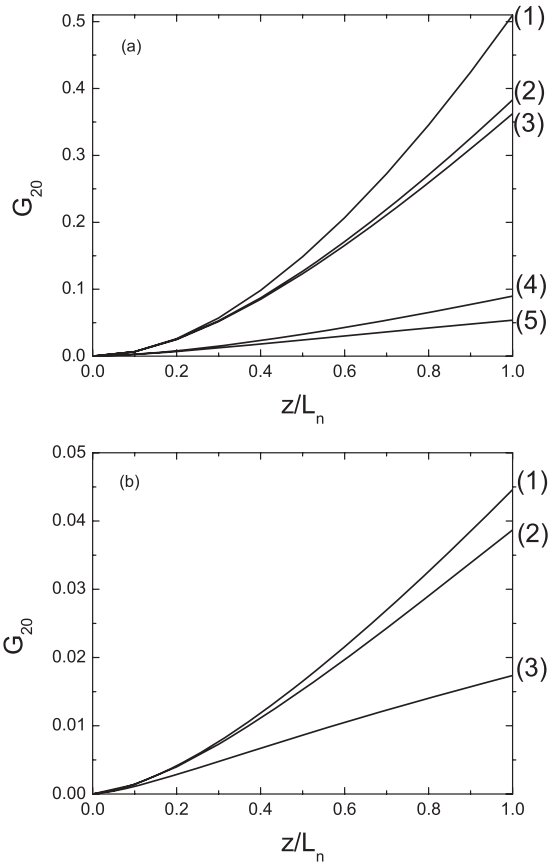

FIG. 1. Dependence of the spectral radiance of the second harmonic radiation on the propagation length. $L_n = 2$ cm, $a = 0.1$. (a) b_1: 0.001 (1), 0.01 (2,3), 0.05 (4,5). b_0: 0.0001 (1,2), 0.001 (3), 0.0005 (4). 0.005 (5). (b) $b_1 = 0.1$, b_0: 0.0001 (1), 0.001 (2), 0.01 (3).

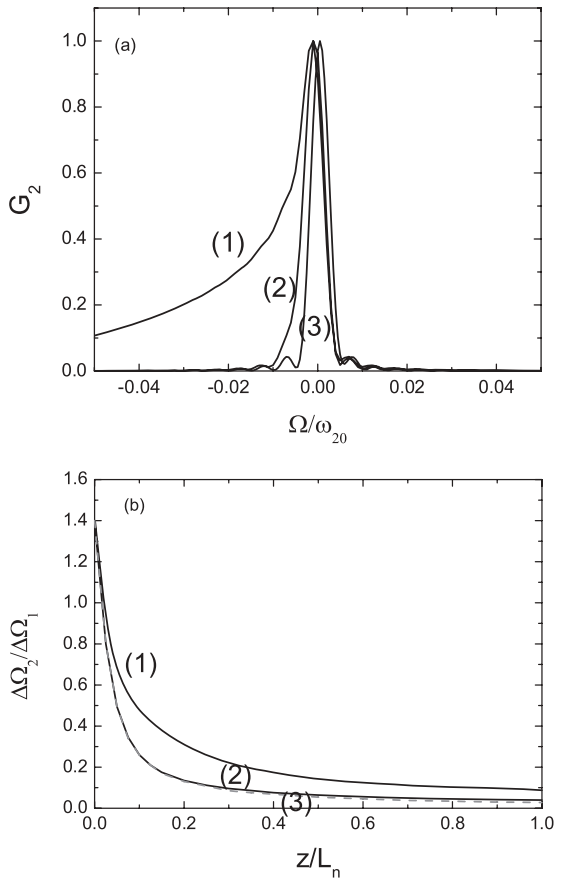

FIG. 2. (a) Frequency spectrum of the second harmonic radiation at $z = 1$ cm. (b) Dependence of the frequency spectrum bandwidth $\Delta\Omega_2$ on the crystal length. $L_n = 2$ cm, $a = 0.1$. $b_0 = 0.0001$, b_1: 0.1 (1), 0.01 (2), 0.001 (3).

$\exp(-\frac{(p_1+p_2)^2}{2\Delta\beta_1^2}) \to \sqrt{\frac{\pi}{2}}\Delta\beta_1\delta(p_1)$, where δ is the Dirac delta function. Then Eq. (13) can be written as

$$G_2(\Omega,p) \approx \frac{(z/L_n)^2}{\sqrt{\pi}\Delta\Omega_1}\exp\left(-\frac{\Omega^2}{2\Delta\Omega_1^2}-\frac{p^2}{2\Delta\beta_1^2}\right) \times \int_{-\infty}^{\infty}\mathrm{sinc}^2 F(\Omega_1,\Omega)\exp\left(-2\frac{\Omega_1^2}{\Delta\Omega_1^2}\right)d\Omega_1, \tag{18}$$

where

$$F = \alpha\left(\frac{g_{10}}{k_{10}}\Omega_1^2 + h(\Omega)\right), \tag{19}$$

and $\alpha \sim z$. In this case, the SH frequency bandwidth only depends on the dispersion properties of the nonlinear crystal and propagation length. It means that noncollinear interactions can be neglected. The influence of the GS model beam envelope diffraction on the frequency bandwidth of the SH radiation increases with an increase in the parameter μ, Fig. 3, curves 2 ($\mu = 0.05$) and 3 ($\mu = 5$) at $z/L_n = 0.5$. The diffraction causes a significant narrowing of the SH frequency spectrum, compare curves 1 and 3 [Fig. 3(b)]. At $\mu \gg 1$ we have $\alpha \gg 1/b_0^2 \gg 1/b_1^2$, and the integral (13) can be significantly simplified

$$G_2(\Omega,p) \approx \frac{2(z/L_n)^2}{\pi^{3/2}\Delta\Omega_1\Delta\beta_0\Delta\beta_1}\exp\left(-\frac{\Omega^2}{2\Delta\Omega_1^2}-\frac{p^2}{2\Delta\beta_1^2}\right) \times \int_{\Omega_1}\left|\int_{p_1}\mathrm{sinc}F_1\exp\left(i\alpha\frac{p_1^2}{k_{10}^2}\right)dp_1\right|^2 \times \exp\left(-\frac{2\Omega_1^2}{\Delta\Omega_1^2}\right)d\Omega_1. \tag{20}$$

An analysis of Eq. (20) shows that the main contribution of $\mathrm{sinc}F_1$ to the integral is obtained at $p_1 \approx 0$ and, as a result, we find

$$G_2(\Omega,p) = \frac{2(z/L_n)^2}{\sqrt{\pi}\Delta\Omega_1\alpha b_1 b_0}\exp\left(-\frac{\Omega^2}{2\Delta\Omega_1^2}-\frac{p^2}{2\Delta\beta_1^2}\right) \times \int_{-\infty}^{\infty}\mathrm{sinc}^2 F(\Omega,\Omega_1)\exp\left(-\frac{2\Omega_1^2}{\Delta\Omega_1^2}\right)d\Omega_1, \tag{21}$$

where $F(\Omega,\Omega_1)$ is given by Eq. (19). So, at $\mu \gg 1$ the profile of the SH frequency spectrum is the same as in the case of the SH excited by a fundamental beam of high spatial coherence ($b_1 \to 0$), see Eq. (18) and curve 3 in both Figs. 2(a) and 3(a). This means that the noncollinear interactions are suppressed by the beam envelope diffraction. On the other hand, the spectral

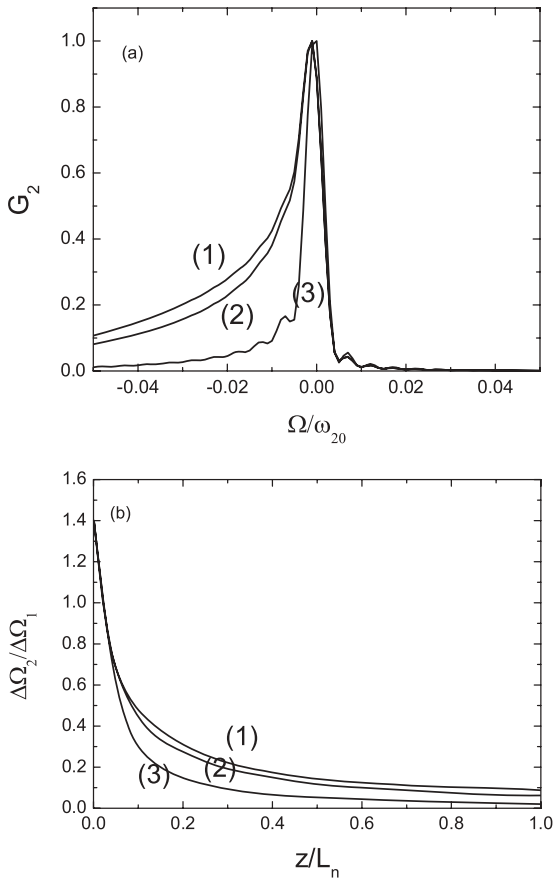

FIG. 3. (a) Frequency spectrum of the second harmonic radiation at $z = 1$ cm. (b) Dependence of the frequency spectrum bandwidth on the crystal length. $L_n = 2$ cm, $a = 0.1$. $b_1 = 0.1$, b_0: 0.0001 (1), 0.001 (2), 0.01 (3).

radiance is reduced by a factor of $v = \alpha b_1 b_0/2$. For $z/L_n = 0.5$ and $b_1 = 0.1$, $b_0 = 0.01$ we find $v \approx 25$, compare curves 1 [Fig. 1(a)] and 3 [Fig. 1(b)] at $z/L_n = 0.5$.

The influence of the GS model beamwidth on the SH frequency bandwidth can be explained by an analysis of the properties of the incoherent fundamental wave under propagation. Making use of Eqs. (5) and (7a) the correlation function of the spectral amplitudes $a_1(\Omega, p)$ can be written as

$$\langle a_1(\Omega_1, p_1) a_1^*(\Omega_2, p_2)\rangle = \langle a_{10}(\Omega_1, p_1) a_{10}^*(\Omega_2, p_2)\rangle \exp\left(i\alpha \frac{p_1^2 - p_2^2}{k_{10}^2}\right). \quad (22)$$

The subsequent calculation of the correlation function of the field $A_1(t,x)$ gives

$$\langle A_1(t_1,x_1) A_1^*(t_2,x_2)\rangle = \frac{a_0^2}{\sqrt{1+\delta^2}} \exp\left(-\frac{(t_2-t_1)^2}{\tau^2}\right) \exp\left(-\frac{(x_1+x_2)^2}{4d_0'^2}\right) \times \exp\left(-\frac{(x_2-x_1)^2}{d_1'^2}\right) \exp\left(-\frac{i\left(x_1^2 - x_2^2\right)\alpha b_1^2}{d_0'^2}\right), \quad (23)$$

where $d_1' = d_1\sqrt{1+\delta^2}$, $d_0' = d_0\sqrt{1+\delta^2}$. In comparison with the input fundamental wave [Eq. (4)] the correlation radius as well as the beamwidth is increased by a factor of $\sqrt{1+\delta^2}$ [13]. At $\delta \gg 1$ we have $d_0' \approx d_0\delta$, $d_1' \approx d_1\delta$ and $\frac{\alpha b_1^2}{d_0'^2} \approx \frac{1}{d_0^2\mu}$. As a result, the influence of the beam envelope diffraction on the SH frequency bandwidth with the increase of δ gradually disappears. Simultaneously the spatial coherence of the fundamental wave increases. In this case at $\mu \gg 1$ the bandwidth of the SH frequency spectrum becomes the same as in the case of the SH excited by a fundamental beam of high spatial coherence.

V. INTENSITY OF THE SECOND HARMONIC RADIATION

We define the intensity of the SH radiation as $I_2 = \langle |A_2(t,x)|^2\rangle$. Then, calculating it at $x = t = 0$, normalizing to the intensity of first harmonic $I_{10} = \langle |A_1(0,0)|^2\rangle = a_0^2$ and making use of Eq. (10) we find

$$\frac{I_{20}}{a_0^2} = \frac{1}{16\pi^4 a_0^2} \int_\Omega \int_p \int_{p'} \langle a_2(\Omega, p) a_2^*(\Omega, p')\rangle d\Omega dp dp', \quad (24)$$

where $I_{20} = I_2(0,0)$. The dependence of the intensity I_{20} on the propagation length z in a nonlinear medium was obtained by the numerical calculation of Eq. (24) and is presented in Fig. 4. As earlier in Sec. IV the same quantities α, b_0, b_1, r, δ, and μ were used. The integral (24) can be simplified for $h(\Omega) \approx -\frac{v\Omega}{k_{10}}$, Eq. (10), when the diffraction of the fundamental beam envelope is neglected ($\mu \ll 1$). As a result, we find

$$\frac{I_{20}}{a_0^2} = \frac{2}{\pi} \frac{(z/Ln)^2}{\sqrt{(1+\gamma^2)(1+\delta^2)}} \int_{-\infty}^{\infty}\int_{-\infty}^{\infty} \frac{\exp\left(-\xi^2\left[1+\delta^2/\left(4R_2^2\right)\right] - \eta^2 - \frac{\kappa^2\alpha^2 b_1^4}{2(1+\gamma^2)}(\xi^2 - r^2\eta^2)^2\right)}{R_2(\xi,\eta)} d\xi d\eta, \quad (25)$$

where $R_2(\xi,\eta) = \sqrt{1 + \frac{\kappa^2\delta^2}{2(1+\gamma^2)}[(\gamma^2+3/2)\xi^2 - r^2\eta^2/2]}$, $\gamma = 2\kappa\frac{z}{L_v}$, and $L_v = \frac{\tau}{|v|} = \frac{\lambda_{10}}{\pi a c|v|}$ is the correlation length of the interaction. For an LBO crystal at $\lambda_{10} = 1.1$ μm we have $c|v| = 0.011$ and $L_v = 0.29$ mm at $a = 0.1$. In the limit case $z \to 0$ ($\alpha \to 0, \delta \to 0, \gamma \to 0, R_2 \to 1$) we find $\frac{I_{20}}{a_0^2} \approx 2(\frac{z}{L_n})^2$, and the dependence of the SH intensity on the propagation length is quadratic. The conversion efficiency of the SH beam is increased up to a factor of 2, as compared to a coherent beam [6]. When $\gamma \gg 1, \delta \ll 1$, then $R_2 \approx 1$. If $\varepsilon_3 = \frac{\kappa^2\alpha^2 b_1^4}{2\gamma^2} \ll 1$, the integration in Eq. (25) gives $I_{20}/a_0^2 \approx 2(\frac{z}{L_n})^2/\gamma$. The intensity varies linearly with z and does not depend on b_0 and b_1. This situation corresponds to curve 1 in Fig. 4(a). When $\varepsilon_3 \gg 1$, the integration in Eq. (25) gives $\frac{I_{20}}{a_0^2} \approx \frac{2^{1/4}\Gamma(\frac{1}{4})(z/L_n)^2}{b_1\sqrt{\pi\kappa\alpha\gamma}} \sim \frac{z}{b_1}$. In this case the intensity decreases with the increase of a parameter

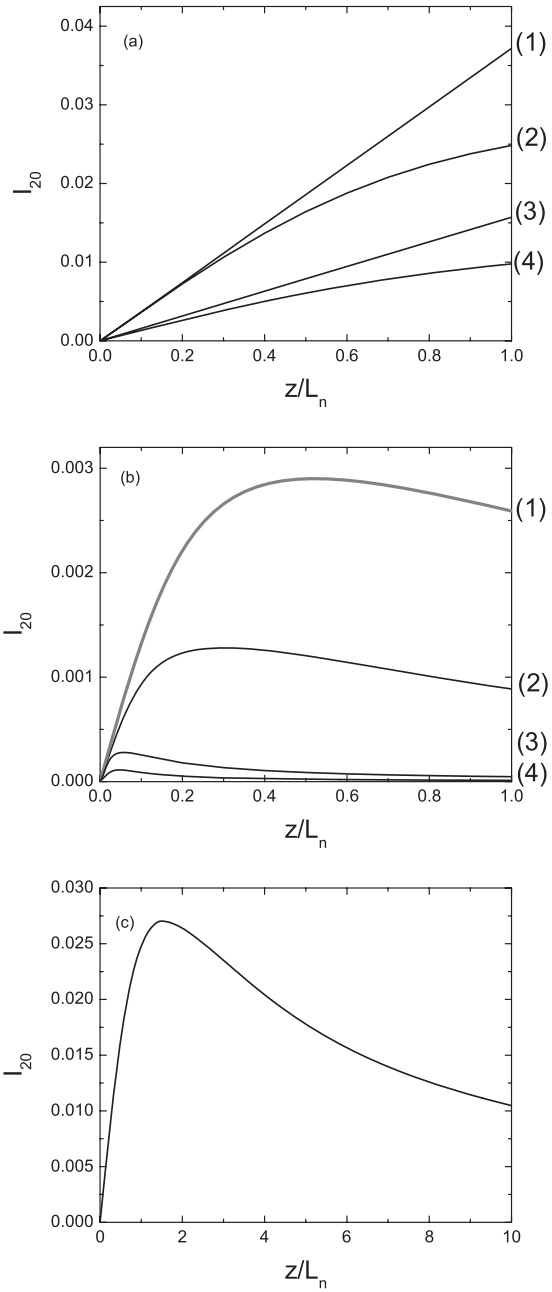

FIG. 4. Dependence of normalized to a_0^2 intensity of the second harmonic radiation on the propagation length. $L_n = 2$ cm, $a = 0.1$. (a) b_1: 0.01 (1,2), 0.1 (3,4). b_0: 0.00001 (3), 0.0001 (1,4), 0.001 (2). (b) $b_1 = 0.1$, b_0: 0.0005 (1), 0.001 (2), 0.005 (3), 0.01 (4). (c) $b_1 = 0.01$, $b_0 = 0.001$.

b_1. That is typical for curve 3 in Fig. 4(a). For $\gamma \gg 1$, $\delta \approx 1$, and $\varepsilon_3 \ll 1$ we find $\frac{I_{20}}{a_0^2} \approx \frac{2(z/L_n)^2}{\gamma\sqrt{(1+\delta^2)(1+\delta^2/4)}}$, and the increase of the intensity I_{20} with z becomes slower, Fig. 4(a), curve 2. In this case, the dependence of the intensity on the beamwidth of the fundamental wave via the parameter δ appears. The typical variation of the SH intensity with propagation in a nonlinear medium for $\delta \gg 1$ is shown in Figs. 4(b) and 4(c). First, at $\delta \ll 1$ the intensity varies with z linearly, and afterwards at $\delta \gg 1$ a saturation of the intensity is observed, and finally, the intensity decreases. This decrease in SH intensity is caused by significant narrowing of the SH spectrum due to diffraction of the beam envelope, Fig. 3.

VI. NUMERICAL SIMULATIONS OF THE NONLINEAR COUPLING EQUATIONS

To control the conditions of low conversion efficiency, the Eqs. (1a) and (1b) were solved numerically without the omission of the nonlinear term in Eq. (1a). The Fourier split-step method [16] was implemented. The equations were simulated M times and averaged values were found. The

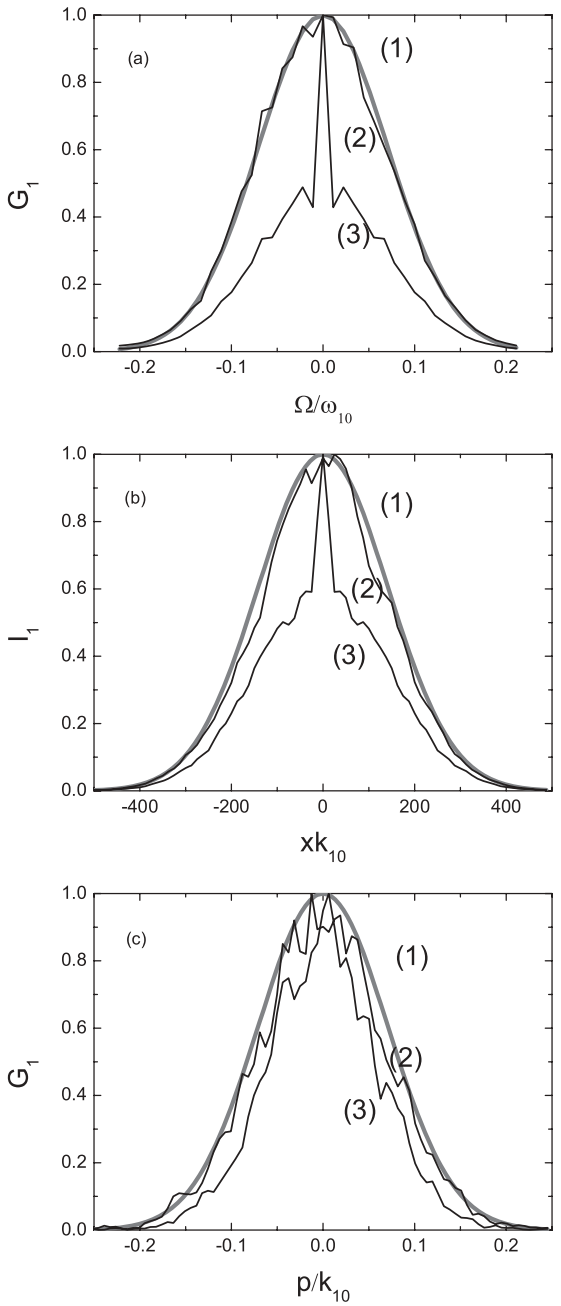

FIG. 5. (a) Normalized to peak value frequency spectrum, (b) intensity profile, and (c) angular spectrum of the fundamental wave. Curve 1, gray line: theoretical curve, curve 2: with random phases, curve 3: without random phases. $a = 0.1$, $b_1 = 0.1$, $b_0 = 0.01$. $T = 20\sigma_t$, $\overline{N} = 10$. Average of $M = 500$ simulations.

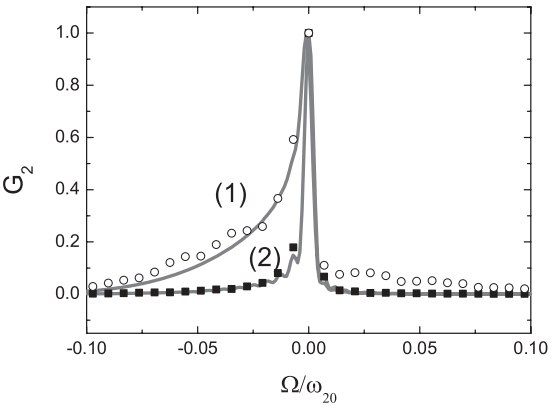

FIG. 6. Frequency spectrum of the second harmonic radiation. Circles and squares: numerical simulation of Eqs. (1), gray lines: Eq. (13). $z = 1$ cm, $L_n = 2$ cm. $a = 0.1$, $b_1 = 0.1$. b_0: 0.0001 (1 and circles), 0.01 (2 and squares). Average of $M = 100$ simulations.

modified method of Ref. [17] was used for the simulation of the input GS model beam with a broad frequency spectrum. We note that the method which is described by the authors of Ref. [17] is only suitable for a narrowband wave. In our case, the frequency band is broad, $a = 0.1$. So, we made some modifications of the method. The field of the input fundamental wave was given as

$$A(x,t) \propto \sum_{j=1}^{N} \Lambda(x,t-t_j)\exp(iK_j x + i\varphi_j). \tag{26}$$

The random phase φ_j was included into consideration, which was absent in Ref. [17]. N is the number of pulses which arrive at random times t_j in the interval $[-T/2,T/2]$. The number N is dictated by Poissonian statistics

$$p(N) = \frac{\overline{N}^N}{N!}\exp(-\overline{N}), \tag{27}$$

where $\overline{N}$ is the average number of pulses in the interval. K_j are random numbers which obey the Gaussian distribution

$$P(K) = \exp\left(-\frac{K^2}{\Delta\beta_1^2}\right). \tag{28}$$

Its variance corresponds to the correlation radius of the beam $d_1 = 2/\Delta\beta_1$. $\Lambda(x,t)$ is factorized into spatial and time parts

$$\Lambda(x,t) = \exp\left(-\frac{x^2}{\sigma_x^2}\right)\exp\left(-\frac{t^2}{\sigma_t^2}\right), \tag{29}$$

where $\sigma_x = \sqrt{2}d_0$ and $\sigma_t = \tau/\sqrt{2}$.

The calculated frequency spectrum, intensity profile, as well as the angular spectrum of the fundamental wave for $a = 0.1$ are presented in Fig. 5. The curves labeled 3 correspond to the method of the authors of Ref. [17] and the curves 2 to the modified method. As we can see the last curves fit the theoretical Gaussian profiles well, which are given by Eqs. (4) and (5).

The frequency spectra of the SH radiation obtained by numerical simulations of Eqs. (1a) and (1b) are presented in Fig. 6. The spectra are compared to the ones obtained by Eq. (13), which are also presented in Fig. 3(a), and a good agreement was obtained.

VII. CONCLUSION

The SH radiation generated in a nonlinear crystal by a GS model beam with a broad frequency spectrum was analyzed. It is revealed that the frequency spectrum of a SH wave depends on the propagation length as well as on the bandwidth of the angular spectrum and beamwidth of the fundamental wave. With a rather small propagation distance, the SH frequency bandwidth increases with an increase in the bandwidth of the angular spectrum of the fundamental wave. This is caused by noncollinear phase matching of the various frequency components in the case of a broad angular spectrum. With an increase in the propagation distance, diffraction of the fundamental beam envelope takes place, and a significant narrowing of the SH frequency spectrum occurs. On the other hand, the bandwidth of the SH angular spectrum is increased by a factor of $\sqrt{2}$ in comparison with the bandwidth of the angular spectrum of the fundamental wave and does not depend on the propagation length. This is a typical case for noncritical type-I phase matching.

The spectral radiance of an SH wave increases with its propagation in a nonlinear medium. The variation of SH intensity is rather complicated. First, the SH intensity increases with its propagation. Afterwards, the diffraction of the fundamental beam envelope takes place and as a result saturation and a decrease in SH intensity are observed. This is caused by a narrowing of the SH frequency spectrum under propagation.

The modified method of the authors of Ref. [17] was implemented for the simulation of an input GS model beam with a broad frequency spectrum. A good agreement between the results of the numerical simulations of Eqs. (1a), (1b), and (13) was obtained.

[1] D. H. McMahon and A. R. Franklin, J. Appl. Phys. **36**, 2073 (1965).
[2] D. H. McMahon and A. R. Franklin, J. Appl. Phys. **36**, 2807 (1965).
[3] D. H. McMahon, J. Appl. Phys. **37**, 4832 (1966).
[4] G. Tamošauskas, Opt. Commun. **284**, 5376 (2011).
[5] N. A. Ansari and M. S. Zubairy, Opt. Commun. **59**, 385 (1986).
[6] M. S. Zubairy and J. K. McIver, Phys. Rev. A **36**, 202 (1987).
[7] M. Zahid and M. S. Zubairy, Opt. Commun **76**, 1 (1990).
[8] A. Picozzi and M. Haelterman, Phys. Rev. Lett. **86**, 2010 (2001).
[9] A. Picozzi, C. Montes, and M. Haelterman, Phys. Rev. E **66**, 056605 (2002).

[10] A. Picozzi and P. Aschieri, Phys. Rev. E **72**, 046606 (2005).
[11] A. Piskarskas, V. Pyragaite, and A. Stabinis, Phys. Rev. A **82**, 053817 (2010).
[12] A. Stabinis, V. Pyragaite, G. Tamošauskas, and A. Piskarskas, Phys. Rev. A **84**, 043813 (2011).
[13] L. Mandel and E. Wolf, *Optical Coherence and Quantum Optics* (Cambridge University Press, Cambridge, England, 1995).
[14] S. A. Akhmanov, V. A. Vysloukh, and A. S. Chirkin, *Optics of Femtosecond Laser Pulses* (American Institute of Physics, New York, 1992).
[15] D. N. Nikogosyan, *Properties of Optical and Laser-Related Materials. A Handbook* (Wiley, Chichester, England, 1997).
[16] G. P. Agrawal, *Nonlinear Fiber Optics* (Academic Press, San Diego, CA, 1989).
[17] G. Gbur, Opt. Express **14**, 7567 (2006).